The high-index surface—a superlattice for two-dimensional electrons

V. A. Volkov, V. A. Petrov, and V. B. Sandomirskiĭ

Institute of Radioengineering and Electronics, Academy of Sciences of the USSR, Moscow
Usp. Fiz. Nauk **131**, 423–440 (July 1980)

A review is given of low-temperature studies of the properties of the two-dimensional electron gas in inversion layers on high-index Si surfaces. The long crystallographic periods associated with such surfaces produce the superlattice effect in the spectrum of the quasi-two-dimensional electron gas. The kinetic coefficients are found to exhibit singularities when the Fermi level and minigaps cross. This was established by measuring the static and the high-frequency conductivities, the Shubnikov-de Haas oscillations, the photoresistivity, the emission of thermal electrons, and the cyclotron resonance in n-type inversion layers near (001) for electron concentrations in the range $10^{12}-10^{14}$ cm^{-2}. The minigap width varies from 1 to 20 meV, depending on the electron concentration. The position of the minigaps in K-space (but not their size) is in quantitative agreement with theory.

PACS numbers: 73.20.Cw, 73.25. + i

CONTENTS

1. Introduction 375
2. Basic information on the two-dimensional electron gas in inversion layers on Si(001) 375
3. Introduction to the theory of orientational superlattices 376
4. Experimental data for inversion layers on high-index silicon surfaces 379
   a) Static electrical conductivity 379
   b) Phenomena in strong magnetic fields 380
   c) Optical properties in the infrared 381
5. Size of minigaps. Discussion of results 383
6. Conclusions 384
7. Addendum 384
References 385

1. INTRODUCTION

There has recently been considerable renewed interest in the studies begun more than ten years ago of the properties of two-dimensional (2D) electron and hole gases in the inversion layers that appear due to strong band bending on a semiconductor surface. This increased activity is evidenced by international conferences held in the USA (1975)[1] and in the Federal Republic of Germany (1977).[2] A third conference was held in Japan in 1979.

As a rule, these studies are concerned with metal-dielectric-semiconductor structures. The possibility of a substantial (by two or three orders of magnitude) change in the surface carrier concentration in the inversion layer without a corresponding change in the other parameters of the material offers unique prospects for experimental investigation of the dependence of the energy spectrum on phenomena such as multiparticle interactions, Anderson and Wigner localization, and so on.

A new area of study emerged in 1977, namely, the properties of inversion layers on surfaces of silicon with high Miller indices. Such inversion layers were found[3] to exhibit anomalies in their galvanomagnetic properties, which were interpreted as being due to a surface superlattice of unknown origin. Independently and simultaneously, one of the present authors[4] predicted that the long crystallographic periods on high-index surfaces should lead to superlattice effects in the electron spectrum of the inversion layer. First attempts at a quantitative interpretation of experimental data were undertaken in Ref. 5 and later in Refs. 6 and 7. We shall follow our previous terminology[4] and will refer to the superlattice associated with the inversion layer on a high-index surface as the orientational superlattice.

In contrast to the usual (artificial) superlattices that consist of thin layers of periodically varying composition,[8] in the present case, we have the possibility of being able to control the Fermi level and the spectrum parameters in a single specimen.

The present paper is devoted to this developing field and is largely concerned with a review of experimental facts and, to a lesser extent, with the state of the theory, which is far from complete. Papers published up to July 1, 1979 are covered.

2. BASIC INFORMATION ON THE TWO-DIMENSIONAL ELECTRON GAS IN INVERSION LAYERS ON Si (001)

Experimental studies of orientational superlattices are usually performed on n-type inversion layers (n-IL) on surfaces close to Si (001). Let us, therefore, begin by considering the properties of n-IL on Si (001).

 0038-5670/80/070375-11$01.10 © 1981 American Institute of Physics

The structure shown in Fig. 1a is used in the investigation of such inversion layers. It consists of a metal electrode (gate) separated by a 1000-Å SiO_2 layer from massive p-type silicon. A voltage V_g is applied between the gate and the body of the semiconductor. When the polarity of V_g is as shown in Fig. 1, and the band bending exceeds the forbidden band gap in silicon, a thin conducting layer (n-IL) appears on the surface of the semiconductor (Fig. 1b). The thickness of this layer is $d \sim 50$ Å and the thickness of the space-charge layer (depletion layer) separating the IL from the rest of the system is $d_{depl} \sim 1\ \mu$. The presence of the high-resistivity depletion layer enables us to decouple electrically the surface region from the rest of the system. The conductivity of the IL is measured with the aid of two ohmic n^+-contacts with a potential difference V_D maintained between them. The surface density of electrons in the IL can be varied by varying V_g and is given by

$$n_s = \frac{C}{|e|}(V_g - V_t), \tag{1}$$

where C is the capacitance of the SiO_2 layer, e is the charge of the electron, and V_t is the threshold inversion voltage (V_t is determined experimentally by determining the position of the rapid rise in mobility in the field effect at 77 °K). The density n_s can be varied from 10^{10} to 10^{13} cm^{-2} in the n-IL on the silicon surface.

Electrons in the inversion layer move in a potential well formed by the electrostatic potential due to the space charge, on the one hand, and the potential barrier on the Si-SiO_2 boundary, on the other (Fig. 1b). In high-quality structures, the scattering of electrons by the Si-SiO_2 boundary is small, and typical mobilities in the n-IL on silicon lie in the range $\mu \sim 10^3$–10^4 cm^2 V^{-1} sec^{-1} at helium temperatures.

Because of the quantization of the transverse component of the quasi-momentum, the electron spectrum of the inversion layer consists in this case of a set of 2D subbands (called electrical subbands) and, in the simplest case, has the form

$$\mathscr{E}_{iv}(k_x, k_y) = E_i + \frac{\hbar^2(\mathbf{k}_\parallel - \mathbf{K}_0^{(\parallel)})^2}{2m_\parallel^*}; \tag{2}$$

where the z axis lies along the normal to the inversion layer, $\mathbf{k}_\parallel = (k_x, k_y)$ is the wave vector in the plane of the inversion layer, E_i is the position of the bottom of the

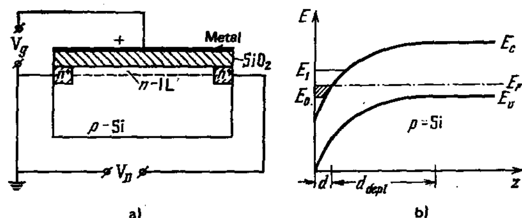

FIG. 1. Metal-dielectric-semiconductor structure (a) and band bending at the surface of the semiconductor (b): V_g-gate potential relative to the semiconductor, V_D-drag voltage, d-thickness of inversion layer, d_{depl}-thickness of depletion layer, $E_c - E_v$-gap width in Si.

i-th electrical subband, v is the number of the valley centered on one of the points $\mathbf{K}_0 = 0.85 \times 2\pi/a\ \langle 001 \rangle$ in the conduction band, $a = 5.43$ Å is the lattice constant of Si, $\mathbf{K}_0^{(\parallel)}$ is the component of $\mathbf{K}_0$ along the plane of the inversion layer, $m_\parallel^*$ is the effective mass in the plane of the inversion layer, which depends on its orientation [for n-IL on Si (001), we have $m_\parallel^* = 0.19\, m_0$, where m_0 is the mass of the free electron], and $\hbar$ is the Planck's constant.

The isoenergy surface in the Si conduction band consists of six ellipsoids of revolution elongated along the cubix axes. In the effective-mass approximation, the ground electrical subband $\mathscr{E}_{0v}$ is doubly degenerate in the valley number ($v = 1, 2$) and consists of two ellipsoids corresponding to the largest effective mass along the normal to the IL. For this case, we have $\mathbf{K}_0^{(\parallel)} = 0$, and the isoenergy profiles are circles. A typical energy gap between the ground and the first excited subbands amounts to a few tens of meV. It follows that only the ground subband is populated at the helium temperatures at which measurements are usually performed. Electrons in this subband form a degenerate 2D gas (or, more precisely, quasi-2D gas).

The density of states per unit area is then independent of energy and is given by

$$D_0 = \frac{g_s g_v m_\parallel^*}{2\pi\hbar^2}, \tag{3}$$

where g_s, g_v are the multiplicities of spin and valley degeneracy, respectively. For n-IL on Si (001), we have $g_s = g_v = 2$ and $D_0 = 1.6 \times 10^{11}$ cm$^{-2}\cdot$ meV^{-1}.

The Fermi energy E_F and the Fermi wave number k_F of a degenerate gas with density of states given by (3) are related to n_s as follows:

$$n_s = D_0 E_F = \frac{k_F^2 g_s g_v}{4\pi}. \tag{4}$$

The above description of the 2D electron gas is largely in agreement with experiment

More detailed accounts of the status of theoretical and experimental studies of inversion layers can be found in the review paper given in Ref. 9 and in conference proceedings.[1,2]

3. INTRODUCTION TO THE THEORY OF ORIENTATIONAL SUPERLATTICES

There is as yet no complete theory of the electron spectrum in inversion layers in high-index surfaces that would be capable of explaining in a unified way all the available experimental data. Nevertheless, some of the basic properties of the spectrum can be determined simply from the 2D-translational symmetry of the system.[4,7,10] We note that there are other approaches to the solution of this problem that are based on other assumptions.[5,6] They will be discussed later.

The wave function of an electron in an inversion layer covers a large number of atomic layers ($d \gg a$; see last Section). Electron-microscopy has shown[11] that, for Si-SiO_2 (119), the crystal lattice in the region of the inversion layer is the same as in bulk if we ignore one

or two possibly damaged atomic layers near the Si-SiO_2 boundary. We therefore assume[4] that the translational symmetry of the electron system is determined by the 2D symmetry of one of the atomic planes of an infinite crystal that are parallel to the surface.

It is clear from Fig. 2 that a long crystallographic period A (superperiod) appears in the inversion layer on the surface of a crystal with high Miller indices. The period A is determined by the particular orientation of the surface and the type of the crystal lattice, and is responsible for the appearance of the superlattice potential. The relative influence of this orientational superlattice on the electron spectrum of the inversion layer will increase as the thickness of the inversion layer is reduced (smaller d/a), i.e., as V_g and n_S increase. It is clear that this influence can be neglected in the "bulk" limit $(d/a \to \infty)$.

Let us now determine the symmetry of one of the atomic planes Si(lmn), where l, m, and n are integers. Its inclination fo the Si (001) plane is defined by the polar angle $\theta = \arccos(n/\sqrt{m^2+n^2+l^2})$ and the azimuthal angle $\varphi = \arccos(l/\sqrt{m^2+l^2})$. We shall suppose that the x,y,z axes lie along $[ln, mn, -l^2-m^2]$, $[-m, l, 0]$, $[l, m, n]$, respectively. As an example, consider the orientation of Si$(11n)$. The silicon lattice consists of two face-centered cubic sublattices shifted relative to each other by a quarter of the space diagonal of the cube. The 2D Bravais lattice is then a simple rectangular lattice for even n and a centered rectangular lattice for odd n. Let us construct the 2D Brillouin band for these two cases. Its dimension along the k_x axis is given by $Q_{min}(\text{even}) = (2\pi/a)\sin\theta$; $Q_{min}(\text{odd}) = (4\pi/a)\sin\theta$, respectively, which is much greater than the usual dimension of the 3D Brillouin band for $n \gg 1$ $(\theta \ll 1)$. In coordinate space, we can introduce the superperiod $A_{even} \equiv 2\pi/Q_{min}(\text{even}) = a/\sin\theta$ for even n and $A_{odd} \equiv 2\pi/Q_{min}(\text{odd}) = a/2\sin\theta$ for odd n, where the x axis serves as the axis of the two-dimensional orientational superlattice. When n changes by unity, this produces a considerable change in the superperiod. This is illustrated in Fig. 2 (cases 1 and 2) by a simple example.

Similarly, we can show that $Q_{min} = 2\pi/A = (\pi/a) \times \sin\theta$ $(\theta \approx 10^\circ, \varphi = 90^\circ)$ for Si(0, 3, 17). These expressions for Q_{min} are useful for comparing with experimental data.

Let us now consider the properties of the electron spectrum in the presence of orientational superlattices.

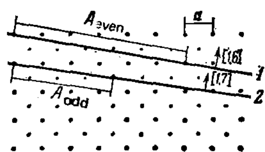

FIG. 2. Section through the crystal lattice by a plane parallel to the inversion layer in the case of a centered square lattice and two different orientations of the surface. A is the long crystallographic period along the inversion layer.

It is well known that even a small superlattice potential produces a radical change in the electron spectrum: it mixes states with wave vectors $\mathbf{k}$ differing by one reciprocal lattice vector, i.e., in this case, by a multiple of Q_{min}. For an electron in the inversion layer with an unperturbed 2D dispersion relation of the form given by (2) (in general, $m_\parallel^*$ in (2) depends on θ and φ but, for $\theta \ll 1$, we may suppose that $m_\parallel^* \approx 0.19 m_0$), the weak potential of the one-dimensional orientational superlattice leads to the appearance of minigaps whose position in $\mathbf{k}_\parallel$-space can be determined from

$$\mathscr{E}_{iv}(k_x, k_y) = \mathscr{E}_{i'v'}(k_x + Q, k_y). \tag{5}$$

Following the generally accepted terminology,[8] we shall refer to resolved 2D bands as minibands. The type of minigap is determined by the indices in (5). So far, the only experimentally confirmed minigaps were those produced by the hybridization of states from the ground electrical subband $(i = i' = 0)$. We shall confine our attention to these minigaps and will omit subband indices i, i'. The general case is considered in Ref. 10.

The hybridization of states in a given valley $(v = v')$ leads to the emergence of "intravalley" minigaps which can appear both in single-valley and many-valley semiconductors.

A particular feature of many-valley semiconductors is the possibility of "intervalley" minigaps (in addition to intravalley minigaps). These are due to the mixing of states from different valleys $(v \neq v')$.

Simultaneous solution of (5) and (2) yields the position of intravalley minigaps in $\mathbf{k}_\parallel$-space:

$$k_x \pm K_0 \sin\theta = \frac{\pi m}{A}, \qquad m = \pm 1, \pm 2, \ldots \tag{6}$$

and the position of intervalley minigaps:

$$k_x = \frac{\pi m}{A}, \qquad m = 0, \pm 1, \ldots \tag{7}$$

where k_x is defined in the expanded-band scheme.

We note that one of the intervalley minigaps is due to $Q = 0$ [$m = 0$ in (7)].

The unperturbed spectrum is doubly degenerate at each point defined by (6) and (7). The superlattice potential removes this degeneracy and leads to the appearance of the miniband spectrum. The minigap $\Delta_{vv'}(Q)$ can be calculated by first determining the form of the effective superlattice potential (see last Section).

The dispersion relation for an electron near a minigap can be found by assuming that it is small and in first-order degenerate perturbation theory given by

$$\tilde{\mathscr{E}} = \frac{\mathscr{E}_v(k_x, k_y) + \mathscr{E}_{v'}(k_x + Q, k_y)}{2} \pm \sqrt{\left[\frac{\mathscr{E}_v(k_x, k_y) - \mathscr{E}_{v'}(k_x + Q, k_y)}{2}\right]^2 + \left|\frac{\Delta_{vv'}(Q)}{2}\right|^2}. \tag{8}$$

It follows from (8) and (2) that the effective mass at the bottom of the second miniband [positive sign in (8)] is proportional to the size of the first minigap and is much smaller than the effective mass at the bottom of

the first miniband, which is equal to $m_{\parallel}^*$.

The above dispersion relation is illustrated in Fig. 3a (in the single-valley case) and in Fig. 4a [two-valley case involving n-IL on Si(11n), where n is odd]. The corresponding isoenergy profiles are shown in Figs. 3b and 4b. We note that Ref. 6 (from which Fig. 4a is taken) makes use of the approach[5,6] in which $Q_{min} = (4\pi/a)\sin\theta$. In the present context, this is valid for Si(11n), where n is odd.

In the single-valley case and small n_s, so that the first miniband ($E_F = E_1$) begins to fill, the Fermi "surface" is close to a circle (broken curve in Fig. 3b). When E_F lies inside the minigap, the closed Fermi "surface" becomes an open surface. As n_s increases still further, E_F enters the second miniband ($E_F = E_2$) and this leads to the appearance of new "lens"-type voids on the Fermi "surface".

The many-valley case, and it is this that is seen in experiment, differs from the preceding case by the fact that, as E_F enters the second miniband (above gap 1 but below gap 2 in Fig. 4a), instead of the open Fermi surface, we have a closed surface resembling the shape of a "dog's bone" (Fig. 4b). In this case, the open surface appears when the Fermi level reaches the next minigap.

Each minigap leads to the appearance of a logarithmic divergence in the density of states $D(E)$ at energies close to the lower edge of the minigap (Fig. 5). This result can be obtained from the formula

$$D(E) = \frac{g_s g_v}{(2\pi\hbar)^2}\frac{\partial S}{\partial E} = \frac{g_s g_v}{2\pi\hbar^2} m_c(E), \quad (9)$$

where $S(E)$ is the area bounded by $\mathscr{E}(\mathbf{k}_{\parallel}) = E$, where $m_c(E) = (1/2\pi)\partial S/\partial E$ is the quasiclassical cyclotron mass. [When the isoenergy surface is not simply connected, a summation must be performed in (9) over all the profiles $\mathscr{E}(\mathbf{k}_{\parallel}) = E$]. It must be remembered that $m_c(E)$ diverges logarithmically as we approach the lower edge of the minigap, whose energy is the saddle point of the dispersion relation (8).[12] The density $D(E)$ differs from zero within the interior of the minigap because the superlattice is one-dimensional. The discontinuity in $D(E)$ at the upper edge of the minigap is connected with the appearance of the contribution due to the second 2D miniband.

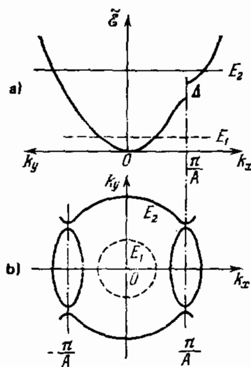

FIG. 3. Dispersion relation (a) and isoenergy profiles (b) for $\mathscr{E} = E_1$ (broken line) and $\tilde{\mathscr{E}} = E_2$ (solid line) in the case of 2D electrons in the presence of 1D superlattice. A is the superlattice period in the single-valley case.

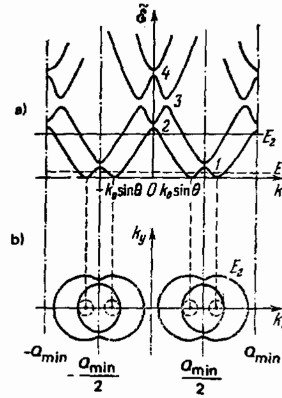

FIG. 4. Dispersion relation (a) and isoenergy profiles (b) in the expanded band scheme in the case of n-IL on Si(11n): n — odd number, $Q_{min} = (4\pi/a)\sin\theta$ is the reciprocal vector of the superlattice, the valleys are centered on the points $k_x = \pm K_0 \sin\theta$; 1, 2, 4 are intervalley gaps, and 3 is an intravalley gap.

In a real system, the singularities in $D(E)$ are smeared out by scattering. Nevertheless, when the size of this effect is less than Δ, the transport coefficients are expected to exhibit singularities as E_F passes through the minigap. The relationships given by (4), which are approximately valid in our case if $\Delta/E_{F0} \ll 1$, can be used to establish the connection between the critical Fermi energy E_{F0}, the density n_{s0}, and the Fermi wave number k_{F0}.

To facilitate comparison with experiment, it is convenient to introduce the "pseudoperiod" of the superlattice as follows:

$$L_{exp} \equiv \frac{\pi}{k_{F0}} = \sqrt{\frac{\pi g_s g_v}{4 n_{s0}}}. \quad (10)$$

Each minigap has its own pseudoperiod L for given A. We emphasize that L is equal to the true period A only for the lower intravalley minigap. For intervalley minigaps, we have $L \neq A$ since k_{F0} in (10) differs from the valley center [compare this with (7), where k_x is measured from the center of the 2D Brillouin zone].

The most complete experimental data are available for the lowest minigap. For n-IL on Si(11n, the properties of the conduction band of silicon [$|\mathbf{K}_0| = 0.85(2\pi/$

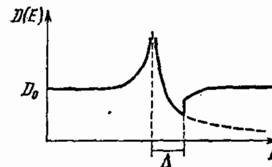

FIG. 5. Density of states in the 2D electron gas in the presence of a 1D superlattice: D_0 is the unperturbed density of states and Δ is the bottom minigap width.

a)] ensure that this is an intervalley minigap lying at $k_x = \pm(2\pi/a)$, which corresponds to $k_{F0} = 0.15(2\pi/a)\sin\theta$. The table lists theoretical[7] and experimental values of L for a number of orientations of the inversion layer.

We emphasize that all the indices of the surface in whose vicinity the inversion layer is produced must be known before $Q_{\min}$ and hence L_{theor} can be calculated. Table I therefore lists only those data for which the Miller indices are known. Thus, for example, the data reported in Ref. 6 are not reproduced because it quotes only the values of θ for the surfaces under investigation.

A different approach to the determination of the position of the minigap in $\mathbf{k}_{\parallel}$-space is developed in Refs. 5 and 6. It is assumed that the reciprocal-lattice surface vector (reciprocal vector of the superlattice in our terminology) can be obtained by projecting the bulk vector $(4\pi/a)[001]$ onto the plane of the inversion layer. This means that $Q_{\min} = (4\pi/a \sin\theta$ does not depend on the complete set of indices of the surface. This procedure gives the correct position of many minigaps in $\mathbf{k}_{\parallel}$-space and, in particular, the values of L_{theor} calculated in this way for the lowest minigap on Si(115), Si(118), and Si(119) [but not Si(2, 2, 23)] agree with those listed in Table I. A critical examination of this approach is given in Sec. 5.

4. EXPERIMENTAL DATA FOR INVERSION LAYERS ON HIGH-INDEX SILICON SURFACES

So far, minigaps have been found in n-IL on surfaces close to Si(001) for θ between 1 and 16° and $\varphi = 45°$, 90°.

Measurements have been carried out on the low-temperature behavior of the static conductivity,[3,6] the Shubnikov-de Haas oscillations,[3,13,14,17] infrared absorption,[5,15,17] photoconductivity,[16] emission of hot electrons,[18] and the behavior of cyclotron resonance[15] as n_S was varied.

The minigap found in the first experimental paper[3] turned out to be of the intervalley type.[5] Intravalley minigaps were examined in Ref. 6.

a) Static electrical conductivity

Figure 6 shows typical results obtained for the conductivities respectively parallel and perpendicular to the superlattice ($\sigma_{\parallel}$ and $\sigma_{\perp}$) as functions of the electron density in the inversion layer in the case of Si (118) ($\theta = 10°$, $\varphi = 45°$). As can be seen, the monotonic growth of $\sigma(n_S)$ has a superimposed structure in the region of 3×10^{12} cm^{-2}, which is due to the crossing of

TABLE I. A—crystallographic period, L—pseudoperiod for the bottom minigap,

$$L_{\text{exp}} = \sqrt{\frac{\pi}{n_{s0}}}, \quad L_{\text{theor}} = \max|2\pi/(Q - 2K_0 \sin\theta)|^{-17}.$$

Surface of	A, Å	L_{exp}, Å	L_{theor} Å
(115)	10	~ 70 [13]	66
(118)	31	101—107 [3]	104
(119)	18	110—120 [5]	116
(2,2,23)	89	~ 200 [13]	223

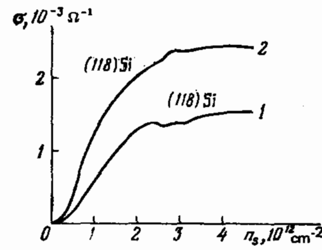

FIG. 6. Conductivity of n-IL on Si (118): $T = 1.7$°K (Ref. 3). 1—Conductivity in the $[88\bar{2}]$ direction (superlattice axis), 2—conductivity along the $[\bar{1}10]$ direction.

the lowest minigap by E_F. This structure is largely determined by the nonmonotonic form of $D(E_F)$ (see Fig. 5), which gives rise to singularities in electron scattering:

$$\sigma(n_s) \sim \tau(E_F) \sim \frac{1}{D(E_F)},$$

where $\tau(E_F)$ is the momentum relaxation time. It follows that $\sigma(n_S)$ exhibits minima at the edges of the minigap, where $D(E)$ is a maximum. The differences between the structures of $\sigma_{\parallel}(n_S)$ and $\sigma_{\perp}(n_S)$ and between their absolute values is connected with the fact that Bragg reflections reduce the velocity of electrons along the super-lattice as compared with the velocity in the perpendicular direction.

The structure of $\sigma(n_S)$ vanishes at $T = 77$°K. This is due to the thermal smearing out of the Fermi level because the mean free path (~1500 Å) is a slowly-varying function of temperature T.

The position of the structure in $\sigma(n_S)$ can be used to determine the pseudoperiod L_{exp} from (10) (see Table I). The only minigap found for Si (118) (see Fig. 6) is the lowest intervalley minigap. Higher gaps have not been found for Si (118) because the values of n_S that are necessary for the Fermi level to reach such gaps are too high ($\gtrsim 1.6 \times 10^{13}$ cm^{-2}, according to estimates in Ref. 7).

Some of these gaps have been found[6] in specimens with lower θ ($\theta = 8.9°; 5.6°; 2.9°; 1.9°; 1.1°$). The orientation of the surfaces was determined by x-ray methods to within less than 0.2°. For such low values of θ, the singularities of $\sigma(n_S)$ are very weak, so that

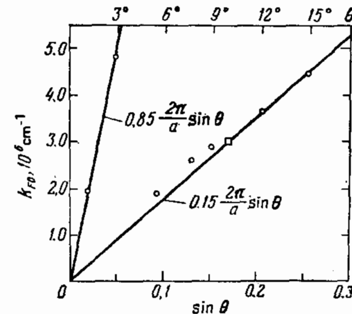

FIG. 7. Angular dependence of the Fermi wave number for which E_F reaches the two minigaps found in Ref. 6. Solid lines—theoretical.[5]

measurements were made of $d\sigma(n_s)/dn_s$ and $d^2\sigma(n_s)/dn_s^2$. Apart from the lowest intervalley minigap (gap 1 in Fig. 4a), two further intervalley minigaps were detected as n_s was increased [$k_{F0}=0.85(2\pi/a)\sin\theta$ and $k_{F0}=1.15(2\pi/a)\sin\theta$]. They correspond to gaps 2 and 4 in Fig. 4a. The lowest intervalley minigap [$k_{F0}=(2\pi/a)\sin\theta$, gap 3 in Fig. 4a] was also detected.

Figure 7 shows data on the position of two minigaps. According to the approach adopted in Refs. 5 and 6, these are the two lowest intervalley minigaps. On the whole, the theory[5,6] is in reasonable agreement with experiment.

The minigap width was determined from the width of the structure in $\sigma(n_s)$. For example, for Si (118), the lowest intervalley minigap was $\Delta=4\pm1$ meV for $n_s \approx 3\times10^{12}$ cm^{-2}, whereas, for Si (115), the result for $n_s\approx 7.5\times10^{12}$ cm^{-2} was $\Delta\approx 18$ meV.

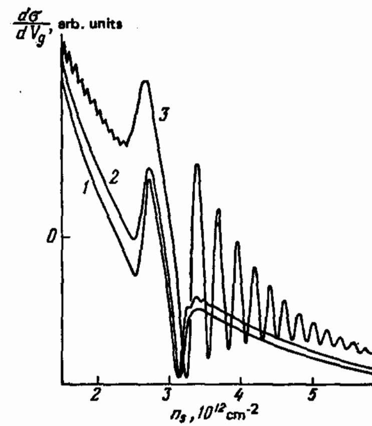

FIG. 8. Shubnikov oscillations in conductivity in the case of n-IL on Si (118): $T=1.5$°K; 1—$H=0$; 2—$H=0.3$ T; 3—$H=0.8$ T (Ref. 3).

b) Phenomena in strong magnetic fields

The Shubnikov-de Haas effect is an important source of information on the electron spectrum of the inversion layer. A particular feature of the inversion layer is that the Shubnikov oscillations in conductivity can be observed not only by varying the magnetic field H (n_s = const), as in the 3D case, but also by varying n_s (H = const). In the latter case, E_F crosses the Landau levels and this leads to conductivity oscillations with the period given by

$$\Delta n_s=\frac{|e|\,g_s g_v H_z}{2\pi\hbar}, \tag{11}$$

where H_z is the component of **H** perpendicular to the surface. The fact that Δn_s is independent of the effective mass is a characteristic property of the 2D system.[9]

Figure 8 shows the function $d\sigma(n_s)/dn_s$ for **H** perpendicular to the surface in the case of Si (118). In nonquantizing fields, $0<H<0.3$ T ($\omega_c\tau<1$, $\omega_c=|e|H/m_c c$, where ω_c is the cyclotron frequency), there are no oscillations. In moderate fields, 0.3 T$<H<$0.7 T, oscillations are observed due to electrons in the second miniband ($n_s>3\times10^{12}$ cm^{-2}), whereas there are no such oscillations in the first miniband (for which $\omega_c\tau<1$).

When $H\gtrsim 0.7$ T, there are oscillations due to electrons in the first miniband ($n_s<3\times10^{12}$ cm^{-2}). Further increase in H extends these oscillations to higher values of n_s and, when $H>0.9$ T, they are superimposed on oscillations due to electrons in the second miniband. This has been interpreted as magnetic breakdown.

The increase in the period of oscillations due to electrons in the second miniband (see Fig. 8) is connected simply with the fact that the total electron density n_s, which is plotted along the abscissa axis, is distributed between the two minibands as the second miniband becomes filled.

If we know the period (11) and the number of oscillations, we can determine the electron density in each miniband. Figure 9, which is taken from Ref. 13, shows the electron density n_{s2} in the second miniband as a function of the total density n_s for a number of orientations. We note that the values of n_{s2} in this figure are too high by a factor of two. In fact, for the intervalley minigap, the multiplicity of the valley degeneracy of the second miniband is 1 and not 2, as was assumed in Refs. 3 and 13 which were based on the single-valley model.

The effective mass at the Fermi level can be obtained from the temperature attenuation of the oscillations (Fig. 10): in the first miniband, $m^*=0.2m_0$ as for Si (001), but, in the second miniband, the mass is much higher and highly nonparabolic. Simple comparison of Figs. 5 and 10 [in the light of (9)] will already show that experiment is in qualitative agreement with theory. Quantitative agreement requires the assumption that Δ in (8) increases substantially with increasing n_s and θ. Thus, for Si (118), the increase in n_s from 3×10^{12} to 6×10^{12} cm^{-2} is accompanied by an increase in Δ from 4 ± 1 to 8 ± 3 meV (Ref. 3).

For Si(2,2,23), the gap Δ cannot be determined since neither the structure of $\sigma(n_s)$ nor oscillations due to electrons lying near the bottom of the second miniband are detectable. This is probably connected with a smearing out process associated with scattering at low values of n_s. Nevertheless, oscillations appear for larger values of n_s and extrapolation of the corresponding curve in Fig. 9 to low values of n_s can be used to obtain the pseudoperiod (see Table I).

Additional information about Δ can be obtained from

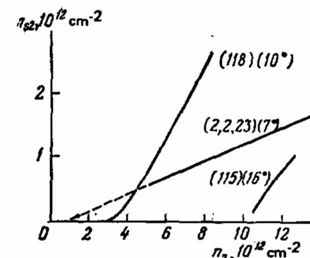

FIG. 9. Population of the second miniband n_{S2} as a function of the total concentration of electrons in n-IL on Si for several orientations.[13] Values of θ are shown in parentheses.

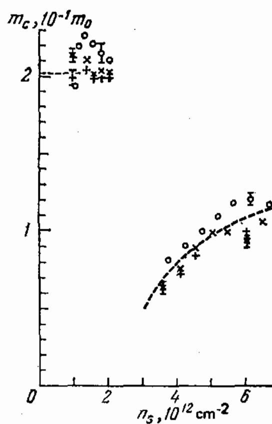

FIG. 10. Shubnikov effective mass in n-IL on Si (118) (Ref. 3).

magnetic breakdown. For values of n_s for which the second miniband begins to fill, and when H is not too high, one can see the Shubnikov-de Haas effect due to electrons in the second miniband with a long period in terms of the reciprocal magnetic field (Fig. 11). In strong fields, i.e., for $H \geq H_0$ [$H_0 \sim 1.2$ T for Si (118), $H_0 \sim 8$ T for Si (115)], magnetic breakdown restores those orbits that were available to the electron in the absence of the minigap (Fig. 11). The condition for magnetic breakdown ($H_0 \sim \Delta^2$) yields $\Delta(115)/\Delta(118) \approx 2.5$, whereas the ratio determined from the period of the Shubnikov oscillations, Δn_s, is equal to 5. One of the reasons for this discrepancy is discussed in the next chapter. In the case of Si(2, 2, 23), the breakdown can be seen for all n_s and H for which the Shubnikov-de Haas effect was observed, which is an indication that Δ is small. For the second minigap (gap 2 in Fig. 4a), very approximate estimates based on magnetic-breakdown data yield[6] $\Delta \sim 10$ meV ($n_s \approx 8 \times 10^{12}$ cm^{-2}, $\theta = 2.90°$) and $\Delta \sim 3$ meV ($n_s \approx 1.7 \times 10^{12}$ cm^{-2}, $\theta = 1.1°$).

In very strong fields (up to 20 T, parallel to the inversion layer, Landau quantization does not occur, and the minibands are subject to spin splitting. This is indicated by the splitting of peaks on the $d\alpha(n_s)/dn_s$

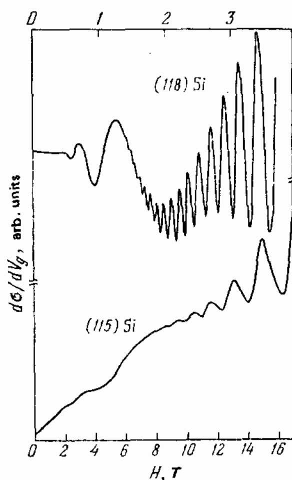

FIG. 11. Effect of magnetic breakdown on the Shubnikov-de Haas effect.[14]

curve.[14] Hence, one can show that, for E_F lying within the minigap, $\Delta(115)/\Delta(118) \approx 2.5$, which is in agreement with the magnetic breakdown result.

There are brief reports on measurements performed on cyclotron resonance in an inversion layer on Si (118) (Ref. 13). When E_F lies below the minigap, cyclotron resonance due to electrons in the first minigap ($m_c \approx 0.2 m_0$) could be observed. As n_s was increased, cyclotron absorption was found to include the contribution due to electrons in the second miniband with lower cyclotron mass. The necessary condition for the observation of cyclotron resonance due to both types of orbit ("lens" and "dog's bone" in Fig. 4b) is that H_z must not be too weak, so that $\omega\tau > 1$ can be satisfied, and not too strong, so that there is no magnetic breakdown. These conditions do not appear to have been satisfied in published work.[13,5]

An anomalous dependence of the amplitude and period of Shubnikov oscillations on uniaxial compression S in the case of Si(1, 1, 10) was recently discovered[17] (Fig. 12). As S increases, the oscillation amplitude initially increases but then falls, whereas, for Si(001), the amplitude monotonically decreases with increasing S. The effect was absent in the case of tension. It is concluded[17] that this anomaly is connected with the dependence of the structure of the miniband spectrum on the magnitude and sign of deformation.

c) Optical properties in the infrared

Infrared absorption data[5,15,17,19] provide us with a direct confirmation of the existence of minigaps. The high-frequency conductivity $\sigma(\omega)$ deduced from these data is shown in Fig. 13 for a given value of n_s. When the electric field $\mathbf{E}_\omega$ in the incident wave is perpendicular to the superlattice axis, the experimental curve is not very different from the usual Drude law (the oscillations are then due to interference effects). However, when the radiation is polarized parallel to the superlattice axis, the $\sigma_\parallel(\omega)$ curve shows an absorption peak which has been interpreted in terms of crossing of the bottom intervalley minigap. The position and height of this peak depend on n_s.

The pseudoperiod of the superlattice was determined from the position of the structure of the static conduc-

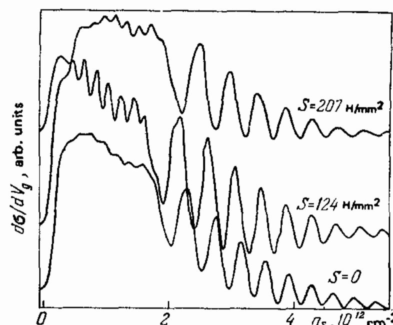

FIG. 12. Shubnikov oscillations in the conductivity of n-IL on Si(1, 1, 10) under pressure S (compression): $H = 3$ T, $T = 1.2$ °K, current flows along the superlattice axis, S is at 45° to the current in the (1, 1, 10) plane.[17]

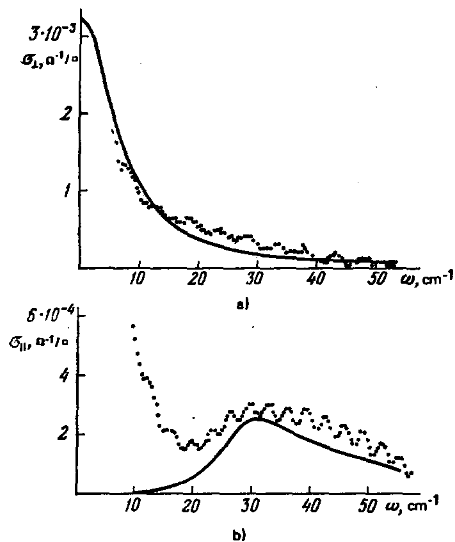

FIG. 13. High-frequency conductivity of n-IL on Si (119) (Ref. 5): $T=1.2$°K, (a) E_ω perpendicular to superlattice axis, (b) E_ω parallel to superlattice axis. Solid line—theoretical[5] ($n_S=2.79\times10^{12}$ cm^{-2}; $\Delta\approx3.4$ meV; $\tau=0.83\times10^{-12}$ sec).

tivity curve $\sigma(n_S)$, and the relaxation time τ was found from the absolute value of $\sigma(n_S)$. Thus, by adjusting Δ until the theoretical and experimental graphs of $\sigma_\parallel(\omega)$ agree, one can determine the function $\Delta(n_S)$ (Fig. 14). The minigap width obtained in this way is an almost linear function of n_S.

Another approach is to investigate infrared absorption in the inversion layer as a function of n_S for $\omega=$ const (Fig. 15). The peak on curve 1 (for the inversion layer with $\theta\approx10°$ and $\varphi=45°$) was absent when the radiation was polarized at right-angles to this superlattice axis, and shifted toward larger n_S as ω was increased. The minigap width determined from these measurements for Si (118) is in agreement with the static conductivity data.

For Si(0, 3, 17) ($\theta\approx10°$ and $\varphi=90°$), there is no peak on curve 2 for either polarization of $\mathbf{E}_\omega$ despite the fact

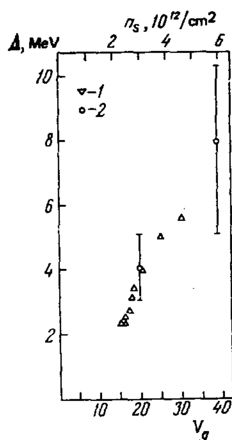

FIG. 14. Width of bottom intervalley minigap as a function of n_S (or V_g, V) as reported in Ref. 5: 1—infrared absorption for Si (119), 2—Shubnikov-de Haas effect data for Si (118).

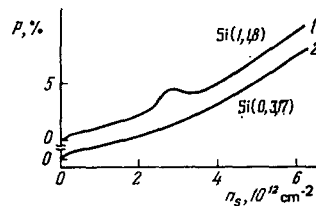

FIG. 15. Relative change in infrered absorption for radiation polarized along the superlattice axis as a function of n_S for two orientations of the inversion layer: 1—$\theta\approx10°$, $\varphi=45°$; 2—$\theta\approx10°$, $\varphi=90°$, $T=1.5$°K, $\hbar\omega=3.68$ meV (Ref. 17).

that the inversion layers for which curves 1 and 2 were obtained had the same mobility and the same value of θ. Nevertheless, the small anisotropy in the derivative of absorption for parallel and perpendicular polarizations relative to this superlattice axis indicates that a small minigap, not exceeding 1 meV, was probably present. Hence, it may be concluded that Δ depends both on θ and on φ.

In addition to the peak on the $\sigma(\omega)$ curve, which is due to the crossing of the minigap, an additional broad peak was observed[19] at high frequencies (~120 cm^{-1}). It was absent when the incident radiation was polarized at right-angles to the superlattice axis, its amplitude increased linearly with n_S, and its position was independent of n_S. The authors of Ref. 19 point out that the frequency range corresponding to this peak also contains the maximum of the density of states for TA phonons. It is suggested that, owing to the properties of the electron-phonon interaction in the superlattice, the TA phonons may become optically active.

The existence of the minigap is reflected even more clearly in photoresponse[6,16] than in static conductivity or absorption. The graph of photoresistance against n_S (Fig. 16) shows a peak (the fourth peak in Fig. 16b) when E_F reaches the bottom minigap. Its position is independent of $\hbar\omega$. The other peaks are the same for both Si (119) and Si (001). The first peak in Fig. 16b is due to heating effects and the second, third, and fifth correspond to transitions between the ground and the three excited electrical subbands.

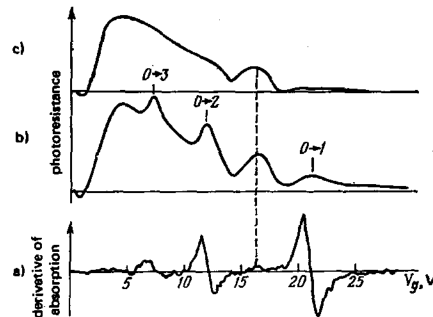

FIG. 16. Photoresponse of n-IL on Si (119) as a function of n_S: $n_S=1.49\times10^{11}(V_g-V_t)$ cm^{-3}; $V_t=0.3$ V; $0\to1$; $0\to2$; $0\to3$—contribution of intersubband transitions; broken line identifies the peak connected with the crossing of the minigap. (a) $\hbar\omega=33.06$ meV; (b) $\hbar\omega=33.06$ meV, $F_D=300$ mV·cm^{-1}; (c) $\hbar\omega=2.50$ meV, $F_D=350$ mV·cm^{-1} (Ref. 16).

Radiative recombination of hot electrons accompanying the crossing of the bottom minigap has been recorded for the structure consisting of a metal (Ti), a 14-Å layer of SiO_2 and Si (119).[18] The electrons were heated by electric field pulses F_D applied along the inversion layer, and emitted radiation with energies $\hbar\omega \approx \Delta$. The power radiated for $\hbar\omega = 4.4$ meV (the detector was tuned to this frequency) and $F_D = 12$ V/cm was 10^{-9} W over an area of 2.5×2.5 mm (linewidth ~1 meV). Estimates show that, by increasing F_D (this is done by increasing the thickness of the SiO_2 film, which determines the maximum value of F_D) and by increasing the area of the structure, the radiated power can be increased to 10^{-6} W. The quantum energy can be varied between 1 and 20 meV. The results of this particular research are of considerable practical interest.

5. SIZE OF MINIGAPS. DISCUSSION OF RESULTS

The position of the minigap in $\mathbf{k}_\parallel$-space is, on the whole, satisfactorily described by existing theories (see Table I and Fig. 7). However, the same can not be said of results concerning the minigap width.

Different workers have established the phenomenological dependence of the bottom minigap width on n_s and θ:

$$\Delta = (B + C \sin^2 \theta)\, n_s, \tag{12}$$

where, according to Ref. 18, $B = 1.1 \times 10^{-12}$ meV·cm^{-2}, $C = 17 \times 10^{-12}$ meV cm^2 (infrared emission by hot electrons corresponding to $\theta = 6°$, 9°; $\varphi = 45°$) and, according to the data reported in Refs. 15 and 17, $B = (1.1 \pm 0.1) \times 10^{-12}$ meV·cm^{-2} and $C \lesssim 10 \times 10^{-12}$ meV·cm^2 (infrared absorption for $\theta = 6°$, 8°, 10°; $\varphi = 45°$).

These data do not indicate a strong dependence of Δ on the azimuthal angle[17]: when $\varphi = 90°$ and $\theta = 10°$, it is found that $\Delta \lesssim 1$ meV for realistic values of n_s. Moreover, the width Δ depends on the type of experiment from which it was deduced. Thus, results obtained from magnetic-breakdown data are very different from those obtained from static conductivity or infrared absorption (see Sec. 4).

Several attempts to calculate the minigap width have been reported.

The theory of intervalley splitting due to scattering by the surface was developed in Ref. 20 for Si (001) and was then generalized[5] for calculations of the bottom intervalley minigap. This minigap is always formed[5] at the point $|k_x| = (2\pi/a)\sin\theta$. The result is given by (12), but the theoretical constants B and C are very much smaller than the experimental values.

Several of the lower minigaps were calculated in Ref. 21 for n-IL on Si surfaces of arbitrary orientation, using the following Hamiltonian of the effective mass method in the expanded band scheme (atomic units):

$$\hat{H} = \begin{pmatrix} \hat{h}_{11} & \hat{h}_{12} \\ \hat{h}_{12}^* & \hat{h}_{22} \end{pmatrix} + V(z), \tag{13}$$

$$\left.\begin{aligned} \hat{h}_{11} &= (\hat{k}_3 - K_0)^2 + M(\hat{k}_1^2 + \hat{k}_2^2), \\ \hat{h}_{22} &= (\hat{k}_3 + K_0)^2 + M(\hat{k}_1^2 + \hat{k}_2^2), \\ \hat{h}_{12} &= \frac{1}{2} E_\Gamma + i(\Sigma e_{12} + N\hat{k}_1\hat{k}_2)\exp\left(i\frac{4\pi}{a}x_3\right); \end{aligned}\right\} \tag{14}$$

where $V(z)$ is the self-consistent IL potential defined in Ref. 9, the (x_1, x_2, x_3) and the (k_1, k_2, k_3) axes lie along the cubic directions [100], [010], and [001], respectively, the principal axes of the IL (x, y, z) are defined in Sec. 3, the constants K_0, M, E_Γ, N are the parameters of bulk silicon, Σ is the deformational potential, and e_{12} is the possible deformation in the (x_1, x_2) plane.

The $\hat{k}\hat{p}$ matrix in (13) describes the dispersion relation for the conduction band of silicon in a direction close to [001] and, in particular, the two valleys with centers at $k_3 = \pm K_0$, $k_1 = k_2 = 0$. The inversion-layer valleys interact in an electric field because of tunneling in $\mathbf{k}$-space. This mechanism of intervalley interaction is referred to as "electrical breakdown" (by analogy with magnetic breakdown). It sets in when the intervalley matrix element of the operator $\hat{h}_{12}$ is different from zero, with the first term in $\hat{h}_{12}$ ensuring "breakdown" through the point Γ in the 3D Brillouin zone of silicon, and the second term ensuring breakdown through the point X. Let us now transform in (13) and (14) to the coordinates x, y, z attached to the inversion layer. It is clear that $\hat{H}$ is invariant under translation in $\mathbf{k}_\parallel$-space by multiples of $(4\pi/a)\sin\theta$ along the k_x axis. The is equivalent to the existence of a one-dimensional superlattice with period $A = a/2\sin\theta$. The position of the minigap in $\mathbf{k}_\parallel$-space as determined in Ref. 21 agrees with the results reported in Refs. 5 and 6.

If we regard $\hat{h}_{12}$ as a perturbation, we can obtain expressions for the minigap width Δ. It has been shown[21,22] that Δ depends on θ, φ, n_s and on k_y and the pressure. For the two bottom minigaps which are of the intervalley type (1 and 2 in Fig. 4a) and are due to "breakdown" through X and Γ, we have in first order in $\hat{h}_{12}$ (in units of 10^{-12} meV·cm^{-2}; $k_y = e_{xy} = 0$):

$$\Delta_X(k_y = 0) = |17.9\alpha \sin 2\varphi \cdot \sin\theta\, \mathrm{tg}\,\theta|\, n_s^*, \tag{15}$$

$$\Delta_\Gamma(k_y = 0) = 0{,}367\alpha(1 + 4.46\sin^2\theta)^2 |\cos\theta|^{-3} n_s^*, \tag{16}$$

where n_s^* is close to n_s under the experimental conditions[21] and $\alpha \approx 0.4$. Higher-lying minigaps, both intervalley and intravalley, are due to interference between the X-breakdown and Γ-breakdown. They appear when higher orders of perturbation theory in $\hat{h}_{12}$ are employed.

Theory[21] predicts strong azimuthal dependence of all the minigaps except for the second (Δ_Γ) because of the presence of the factor $\sin 2\varphi$ in (15). All the minigaps (apart from Δ_Γ) are also found to depend on the size and sign of the deformation. Moreover, since Δ depends on k_y, the values of Δ deduced from magnetic-breakdown data should be appreciably different from those deduced from optical absorption. The above conclusions, given in Ref. 21, are in qualitative agreement with experimental data.[3,17]

However, the numerical values of the minigap widths are, as a rule, much lower than the experimental values.

In our view, the inconsistency of the approaches developed in Ref. 5 (see also Refs. 6 and 21) is that they do not reflect the actual 2D symmetry of the system. It was, in fact, postulated that the minimum surface vector of the reciprocal lattice was always equal to $(4\pi/a)\sin\theta$, whereas, as was shown in Sec. 3, this is valid only for Si(11n) with n odd. In general, the vector $(4\pi/a)\sin\theta$ is one of the vectors of the reciprocal lattice but not necessarily the smallest. If we follow the above papers, we cannot, therefore, deduce, for example, the position of all the minigaps for arbitrary orientation of the inversion layer. This is so, in particular, for the bottom minigap for Si(2, 2, 23) (if we follow Ref. 5, we obtain $L_{\text{theor}} = 149$ Å, which is in worse agreement with experiment than the value reported in Ref. 7, namely $L_{\text{theor}} = 223$ Å).

6. CONCLUSIONS

The existence of minigaps in the case of n-IL on high-index Si planes can thus be regarded as firmly established. The position of the minigaps in $\mathbf{k}_\parallel$-space is qualitatively described by existing theories. On the other hand, calculated values of the minigap width turn out to be too low. It follows that the derivation of a consistent theory of the orientational superlattice still remains a pressing problem.

The final elucidation of the nature of the effective potential of this type of superlattice will have to await more extensive experimental studies (using other orientations and materials, including single-valley semiconductors).

One hopes that such effects will be observed also in other systems, for example, in the 2D electron gas on the cleavage plane of germanium bicrystals.[23]

The ability to control the parameters of the superlattice is important from the applied point of view. In this connection, we note the paper by Tsui and Gornik[18] (see the section on "Experimental Data").

In conclusion, we should like to thank A. A. Sukhanov and E. V. Chenskiĭ, and also B. M. Vul and E. P. Zavaritskaya for useful discussions.

7. ADDENDUM

We shall now summarize the new results published since this review was written. They were reported at the Fourteenth International Conference on the Physics of Semiconductors (England, 1978) and the Third International Conference on the Electronic Properties of 2D Systems (Japan, 1979).

Careful measurements of infrared absorption in n-IL on Si(11n) and Si(01n) at several fixed frequencies[24] have shown that the measured bottom minigap width $\Delta_{\text{exp}}(n_S)$ is a nonlinear function of n_S. This can be explained by assuming that the true minigap width [see Eq. (8)] is linear in n_S but depends on k_y in an essential manner. Therefore, instead of (12), the following empirical formula for the bottom minigap has been proposed

$$\Delta(\theta, \varphi, n_s, k_y) = (A_1 + B_1 f(\theta, \varphi) + C_1 k_y^2)\, n_s, \tag{17}$$

where $A_1 \simeq 0.3\times 10^{-12}$ meV·cm^2; $B_1 = 45\times 10^{-12}$ meV·cm^2; $C_1 = (0.09/\pi)\times 10^{24}$ meV·cm^4; $f(\theta, \varphi) \simeq \sin^2\theta$ for $\theta \lesssim 8°$; $f(\theta, \varphi) \sim \sin 2\varphi$. It is important to note the qualitatively new behavior of $\Delta(\theta)$ for large θ: when $\theta > 8°$, the function $f(\theta)$ reaches a plateau, which is theoretically unexpected. The function $\Delta(k_y, \theta)$ differs from the predictions in Refs. 21 and 22. Moreover, when $\theta = 0$, $k_y = 0$, the value given by (17), in contrast to that given by (12), is in good agreement with experimental data on intervalley splitting in n-IL on Si (001).

The first quantitative determinations of high-lying minigap widths based on infrared absorption[25] and infrared emission by hot electrons[26] have shown that the spectrum emitted as a result of radiative recombination of hot electrons contains peaks (up to four peaks for specimens with $\theta \sim 1°$) due to the crossing of the minigaps Δ_i (the subscripts $i = 1, 2, 3, 4$ label the minigaps in order of increasing energy; see Fig. 4). It has been shown[26] that $\Delta_2(n_S)$ changes from 3.0 to 4.7 meV as n_S increases from 2.5×10^{12} cm^{-2} to 6.9×10^{12} cm^{-2}; Δ_3 increases from 2.3 to 3.2 meV as n_S increases from 3.9×10^{12} to 6.9×10^{12} cm^{-2}; and $\Delta_4 \sim 2.3$ meV when $n_S = 6.9\times 10^{12}$ cm^{-2}. These values are higher than the theoretical predictions[21] by nearly an order of magnitude.

The intrasubband infrared photoconductivity of n-IL on Si (118) has been measured[27] in quantizing magnetic fields. Shubnikov-type oscillations with clear manifestations of magnetic breakdown through the bottom minigap have been found. Experiments on cyclotron resonance in Si (119) have revealed[27] certain features such as the shift, broadening, and complication of line shapes with increasing n_S, for which no interpretation is as yet available.

Some authors[28,29] have noted the dependence of individual results on technological conditions under which the specimens were produced. This refers, above all, to the function $\Delta_1(\varphi)$ for fixed θ. Thus, for $\theta = 10°$, it is found that $\Delta_1(\varphi = 0°) \ll \Delta_1(\varphi = 45°)$, according to Refs. 17 and 24; according to Ref. 28, $\Delta_1(\varphi = 0°) \approx \Delta_1(\varphi = 45°)$; according to Ref. 29, $\Delta_1(\varphi = 0°) = 0.5\Delta_1(\varphi = 45°)$. Several (although not all) specimens with $\theta \sim 1°$ exhibit a new gap[28] when the Shubnikov-de Haas effect is examined, the position of which in $\mathbf{k}_\parallel$-space is not described by the theory.[5,6,21]

All authors emphasize the considerable discrepancy between theory and experiment insofar as the gap width is concerned. It is thought that this may be due to deformations at the Si-SiO_2 boundary, the magnitude of which may depend on fabrication technology.[29] Inclusion of the exchange-correlation interaction may also increase the predicted values of Δ.

Kaplan[30] has contributed an interesting paper in which slow electron diffraction by atomically pure Si surfaces cut at small angles to Si (001) has revealed the presence of ordered steps which do not disappear even when specimens are heated up to 1100°C or when adsorption of hydrogen or oxygen is investigated. The geometric size of these steps is in agreement with

predictions for the perfect high-index surface. This periodic topology may be one of the reasons for the appearance of the superlattices[4,13] provided it does not disappear during the preparation of the metal-dielectric-semiconductor structure.

[1]Proc. Intern. Conf. on Electronic Properties of Quasi-2D Systems, Providence, USA, 1975; Surf. Sci. 58, 1 (1976).

[2]Proc. Second Intern. Conf. on Electronic Properties of 2D Systems, Berchtesgaden, West Germany, 1977; Surf. Sci. **73**, 1 (1978).

[3]T. Cole, A. A. Lakhani, and P. J. Stiles, Phys. Rev. Lett. 38, 744 (1977).

[4]V. A. Petrov: V kn. VI Vsesoyuznoe soveshchanie po fizike poverkhnostnykh yavleniĭ v poluprovodnikakh, Kiev, Noyabr' 1977 (in: Sixth All-Union Conf. on the Physics of Surface Phenomena in Semiconductors, Kiev, November, 1977), Abstracts of Papers, Naukova Dumka, Kiev, 1977, Part 2, p. 80; Fiz. Tekh. Poluprovodn. **12**, 380 (1978) [Sov. Phys. Semicond. **12**, 219 (1978)].

[5]L. J. Sham, S. J. Allen Jr., A. Kamgar, and D. C. Tsui, Phys. Rev. Lett. 40, 472 (1978).

[6]D. C. Tsui, M. D. Sturge, A. Kamgar, and S. J. Allen Jr., *ibid.* 1667.

[7]V. A. Volkov and V. B. Sandomirskiĭ, Pis'ma Zh. Eksp. Teor. Fiz. **27**, 688 (1978) [JETP Lett. **27**, 651 (1978)].

[8]L. Esaki and L. L. Chang, Thin Sol. Films 36, 285 (1976).

[9]F. Stern, in: Surface Science: Recent Progress and Perspectives, Cleveland, CRC Press, 1974 [Russ. Transl., Mir, Moscow 1977, vol. 2, p. 280]

[10]V. A. Volkov and V. B. Sandomirskiĭ, Phys. Status Solidi, B 94, 349 (1979).

[11]O. L. Krivanek, T. T. Sheng, and D. C. Tsui, Appl. Phys. Lett. 32, 437 (1978).

[12]I. M. Lifshits, M. Ya. Azbel', and M. I. Kaganov, Elektronnaya teoriya metallov (Electron Theory of Metals), Nauka, Moscow, 1971, p. 52.

[13]A. A. Lakhani, T. Cole, and P. J. Stiles, Surf. Sci. **73**, 223 (1978).

[14]P. J. Stiles, T. Cole, and A. A. Lakhani, J. Vac. Sci. Technol. **14**, 969 (1977).

[15]T. Cole, J. P. Kotthaus, T. N. Theis, and P. J. Stiles, Surf. Sci. **73**, 238 (1978).

[16]A. Kamgar, M. D. Sturge, and D. C. Tsui, *ibid.* 166.

[17]W. Sesselmann, T. Cole, J. P. Kotthaus, R. Kellerer, H. Gesch. J. Eisele, and G. Dorda, In: Abstracts of Fourteenth Intern. Conf. on Physics of Semiconductors, Edinburgh, 1978, p. 299 (preprint).

[18]D. C. Tsui and E. Gornik, Appl. Phys. Lett. **32**, 365 (1978).

[19]D. C. Tsui, S. J. Allen Jr., R. A. Logan, A. Kamgar, and S. N. Coppersmith, Surf. Sci. 73, 419 (1978).

[20]L. J. Sham and M. Nakayama, *ibid.* 272.

[21]F. J. Ohkawa, J. Phys. Soc. Jpn. **46**, 855 (1979).

[22]F. J. Ohkawa, *ibid.* **45**, 1427 (1978).

[23]B. M. Vul and É. P. Zavaritskaya, Zh. Eksp. Teor. Fiz. **76**, 1089 (1979) [Sov. Phys. JETP **49**, 551 (1979)].

[24]W. Sesselman and J. P. Kotthaus, Solid State Commun. **31**, 193 (1979).

[25]D. C. Tsui, A. Kamgar, and M. D. Sturge, Phys. Semicond. (Inst. Phys. Conf. Ser. Lnd) No. 43, 1335 (1979).

[26]E. Gornik, R. Schawarz, G. Lindemann, and D. C. Tsui, in: Yamada Conf. II on Electronic Properties of 2D Systems (Third Intern. Conf.), Lake Yamanaka, Japan, 1979, Collection of Papers, p. 914.

[27]H. Okamoto, K. Muro, S. Narita, and S. Kawaji, *ibid.* 707.

[28]P. J. Stiles, Phys. Semicond. (Inst. Phys. Conf. Ser., Ldn.) No. 43, 41 (1979).

[29]T. Ando, see Ref. 26, p. 607.

[30]R. Kaplan, Phys. Semicond. (Inst. Phys. Conf. Ser. Lnd.) No. 43, 1351 (1979).

Translated by S. Chomet